Thermal energy storage of molten salt –based nanofluid containing nano-encapsulated metal alloy phase change materials

Nuria Navarrete[1], Rosa Mondragon[1*], Dongsheng Wen[2], Maria Elena Navarro[3], Yulong Ding[3], J. Enrique Julia[1]

[1]Departamento de Ingeniería Mecánica y Construcción, Universitat Jaume I, 12071-Castellon de la Plana, Spain

[2]Birmingham Centre of Energy Storage, University of Birmingham, Birmingham B15 2TT, United Kingdom

[3]Institute of Particle Science and Engineering, University of Leeds, Leeds LS2 9JT, United Kingdom.

Corresponding author: mondragn@uji.es

ABSTRACT

The availability of Thermal Energy Storage systems in Concentrated Solar Power plants makes them suitable to handle the gap between energy supply and power demand. Increasing the total thermal energy storage capacity of the Thermal Energy Storage materials used is of interest to improve their efficiency. In this work the thermal energy storage of the so called solar salt (60% $NaNO_3$ - 40% KNO_3) was improved by adding a phase change material composed of Al-Cu alloy nanoencapsulated with an aluminium oxide layer naturally formed when exposed to oxygen. The resistance of the oxide shell to thermal cycling up to 570ºC and its compatibility with the molten salt were proved. The specific heat and the total thermal energy storage were evaluated at different solid mass loads. Although the specific heat and thus the sensible heat storage decreases with solid content, the contribution of the phase change enthalpy and the latent heat storage can increase the total thermal energy storage up to a 17.8% at constant volume basis comparison. Besides, the thermal conductivity of the nanofluid was increased when adding the nanoparticles improving its heat transfer performance under some particular conditions.

Keywords: thermal storage; nanofluids; phase change enthalpy; specific heat; thermal conductivity

Nomenclature

CSP	Concentrated Solar Power
DSC	Differential Scanning Calorimetry
HTF	Heat Transfer Fluid
LCOE	Levelized Cost Of Energy
LFA	Laser Flash Analysis
PCM	Phase Change Material
nePCM	Nanoencapsulated Phase Change Material
SEM	Scanning Electron Microscopy
TEM	Transmission Electron Microscopy
TES	Thermal Energy Storage

Symbols

α	Thermal diffusivity
c_p	Specific heat
D	Diameter of the pipe
ΔH_f	Phase-change enthalpy
ε_r	Relative error
ϕ	Volume fraction
h	Heat transfer coefficient
k	Thermal conductivity
m	Mass
μ	Viscosity
Mo	Mouromtseff number
Nu	Nusselt number
q	Energy density storage
ρ	Density
T	Temperature
V	Volume
w	Mass fraction

Subscripts

bf	Base fluid
exp	Experimental value
latent	Latent heat

nf	Nanofluid
np	Nanoparticles
sensible	Sensible heat
th	Theoretical value
total	Total energy

1. Introduction

Solar energy is one of the cleanest and cheapest energy resources that can be converted into thermal and electrical energy being eco-friendly. It has become the most important renewable energy source to reduce the consumption of fossil fuels and to mitigate Global Warming [1, 2]. For high temperature applications, the solar radiation needs to be concentrated and the electricity generation can be achieved through Concentrated Solar Power (CSP) plants. One of the features that make CSP plants different from other renewable technologies is the ability to include a Thermal Energy Storage (TES) system in order to handle the intermittencies of solar availability and prevent the gap between energy supply and power demand [3].

Thermal energy storage can be achieved mainly by sensible heat storage and latent heat storage [4]. In sensible heat storage processes there is no phase change happening and materials experience a raise in temperature. The relation between the change in temperature and the stored heat is given by the specific heat of the TES material. In latent heat storage processes, the energy absorbed or released is stored by a phase transition at a constant temperature. TES materials used for latent heat storage are the so called phase change materials (PCMs) and the stored heat is given by the specific latent heat or phase change enthalpy [5-8].

Molten salts are widely used as Heat Transfer Fluid (HTF) and TES materials in Concentrated Solar Power plants (CSP) [9,10]. Solar Salt is the mixture of sodium and potassium nitrates (60/40 wt%. respectively) commonly used in this industry. Its higher decomposition temperature (550-600ºC) compared to that of water or thermal oils, makes it adequate for these high temperature applications, whereas its price is not excessive. However, its thermal properties such as thermal conductivity and specific heat are worse than those of water.

One of the actions gaining attention in the last years to increase the efficiency in the heat transfer and thermal storage systems currently present in these industrial processes is the use of salt-based nanofluids [11,12]. A nanofluid is a stable suspension of solid particles with nanometrical size used as HTF or TES material whose thermal properties have been enhanced [13]. The addition of nanoparticles to a base fluid implies an increment in the thermal conductivity of the nanofluid due to the higher thermal conductivity of the solid. Furthermore, although according to the mixture rule the specific heat of the nanofluid should decrease due to the lower specific heat of the nanoparticles, abnormal enhancements in the specific heat capacity of molten salts and ionic liquids have been reported [14-26]. This enhancement provides an increase in the

sensible heat storage capacity of the TES material thus improving the efficiency of the storage system. The only salt-based nanofluid drawback is the increase in viscosity produced by the addition of the nanoparticles, which can lead to increments in pressure drop when used as HTF in dynamic conditions.

In order to further increase the total heat storage capacity of a TES material the use of nanoencapsulated Phase Change Materials (nePCMs) was proposed [27-31]. To introduce these PCMs as the solid phase in a nanofluid, a core-shell structure is needed so the particles do not collapse into each other when in melted state, losing the advantages associated with their nanometric size. Therefore, nePCMs are composed of a PCM core and a covering shell with high melting temperature, resistant enough to prevent any leakage from the nucleus when it is in liquid state. The addition of a nePCM with high phase change enthalpy, capable of storing and releasing large quantities of energy during its melting and solidification processes increments the total heat storage capacity of the nanofluids compared to the base fluid due to the contribution of the latent heat of the nanoparticles cores.

One of the main drawbacks of the use of nePCMs is the complexity in the synthesis process of the covering shell. The encapsulation of the PCM is achieved usually following a chemical route in which a polymeric or inorganic shell is produced [32, 33]. However, authors have recently proposed the use of self-encapsulated metallic nePCMs [31]. Metals and alloys are used as latent heat storage materials due to their highest heat storage capacity per unit volume and thermal conductivity. The key feature of metals is that they undergo oxidation in contact with air easily. Although this could be considered as a drawback at a first sight, it was observed that the metal oxide nanolayer formed at the nanoparticle surface acts as a natural shell to encapsulate the metallic PCM, avoiding additional steps of encapsulation.

The present work proposes a nanofluid composed of a mixture of molten nitrates as the base fluid (solar salt) and nePCM consisting of Al-Cu alloy nuclei encapsulated by the metal oxide layer that is naturally formed when the nanoparticles are exposed to oxygen. The nePCM has been characterized and the suitability of the oxide shell as encapsulation has been proved for high temperature working conditions similar to those of possible industrial applications. The phase change enthalpy of the nePCM and the specific heat of the nanofluids were measured in order to evaluate the total heat storage capacity (contribution of both sensible and latent storage) for different concentrations of nanoparticles. A maximum enhancement of 10.6% at constant mass basis and 17.8% at constant volume basis was achieved for 10 wt.% of nePCM, demonstrating the improvement of the thermal performance of the fluid when adding the nePCM. Thermal conductivity was also measured and a maximum enhancement of 8.9% was achieved.

2. Materials and methods
2.1 Materials

The nanoparticles used and studied in this work were commercially obtained from Advanced Powder Technologies LLC. They consist on particles of an Aluminium-Copper alloy in an 80%Al-20%Cu weight percentage. They are produced by the wire

explosion in inert gas method, what makes their size distribution wide, presenting particles that can reach from 20 up to 300 nm in diameter.

The base fluid used was a mixture of sodium and potassium nitrates, 60/40 wt.% respectively, commonly known as Solar Salt in the solar energy industry, where it is used as both TES material and HTF.

The nitrates were purchased from Labkem (Analytical grade ACS). They were weighted in the desired proportions and mechanically mixed in the laboratory with a mill. Any trace of humidity was previously removed by putting the nitrates in an oven at 100ºC for 20 min.

Nanofluids consisting of Solar Salt and Al-Cu nanoparticles with mass loadings of 0.5%, 1%, 1.5%, 5% and 10% were prepared. For that purpose, the nanoparticles were added to the previously mixed nitrates and mechanically blended. The commonly used dissolution method was avoided to prevent the full oxidation of the metallic nanoparticles cores.

2.2 Characterization of Al-Cu nanoparticles

In order to fully characterize the Al-Cu nanoparticles, images were taken with a Transmission Electron Microscope (TEM, JEOL-JEM 2100) and a Scanning Electron Microscope (SEM, JEOL-JSM 6510). Analyses of these images were made to determine the morphology and size distribution of the nanoparticles, as well as the thickness of the encapsulating shell. The structure and chemical composition of the core and shell were studied using the same microscope, which includes High-Resolution and EDX (Oxford INCA) analysis modules.

Information of the phase change processes, such as the melting and crystallisation temperatures, phase change enthalpies, and their evolution through thermal cycling was obtained by Differential Scanning Calorimetry analysis (DSC, DSC2 Mettler Toledo). A sample of around 13mg of nanoparticles was analysed in a 40µl aluminum crucible. 150 thermal cycles from 460ºC to 570ºC were performed under nitrogen atmosphere (25 mL/min N_2 flow rate), with 20 K/min heating and cooling rates and 5 minutes isotherms at the maximum and minimum temperatures. More detailed analyses were performed every 20 cycles with the same characteristics but heating and cooling rates of 5 K/min, in order to obtain more accurate values of the melting and crystallisation temperatures and enthalpies.

The specific heat of the nanoparticles was also measured by means of DSC tests. The method used was the areas method, which has been checked to provide better results than the dynamic or isostep methods [34]. In this method, a standard sapphire and the sample were submitted to consecutive isothermal segments with a 1ºC step and no heating stages amid. The DSC signal provided a peak, whose area was used to calculate the specific heat. Temperature steps were applied at 300ºC, 350ºC and 400ºC, with 5 minute isotherms before and after the step. Tests were also carried out at a constant 25 mL/min N_2 flow rate. To ensure repeatability at least three samples were prepared. For each one, two cycles were run in order to obtain a mean value.

2.3 Characterization of the nanofluids

A similar DSC analysis to that of the nanoparticles was performed over the nanofluid with Al-Cu at 10 wt.% using the same crucible. A sample of around 21 mg was submitted to 55 thermal cycles from 460ºC to 570ºC under nitrogen atmosphere, with 20 K/min heating and cooling rates and 5 minutes isotherms at the maximum and minimum temperatures. 5 slow cycles in between to better observe the behaviour and evolution of the nanoparticles immerse in Solar Salt were performed at 5 K/min heating and cooling rates.

The specific heat of the nanofluids was also measured following the same procedure stablished for the nanoparticles. The areas method was used with 1ºC step at 300ºC, 350ºC and 400ºC, with 5 minute isotherms before and after the step. At least three samples of each nanofluid were prepared and two cycles were run for each one in order to obtain a mean value. The experimental error of the mean value was statistically obtained at a 95% of confidence level, with a mean error of 3.96% at 300ºC, 4.62% at 350ºC and 5.60% at 400ºC.

Thermal diffusivity was also measured by means of Laser Flash Analysis (LFA, LFA427, Netzsch). In the LFA measurement, the diffusivity was determined by heating the front face of the sample by a laser with simultaneous record of the temperature profile on the rear face. Samples of around 91 mg where analysed in a platinum sample holder. The holder was previously coated with graphite to increase the absorption and emission of radiation. Thermal diffusivity was measured at 300ºC under nitrogen atmosphere.

Thermal conductivity of the nanofluids was calculated from these measurements using Equation 1:

$$k = \alpha \cdot \rho \cdot c_p \tag{1}$$

where k is the thermal conductivity, α is the thermal diffusivity, c_p is the specific heat and ρ is the sample density which can be calculated from the mixture rule:

$$\rho = (1 - \phi) \, \rho_{bf} + \phi \, \rho_{np} \tag{2}$$

where ϕ is the volume fraction, and ρ_{np} and ρ_{bf} are the densities of the nanoparticles and the base fluid respectively.

The density of the molten solar salt was obtained from literature [9]:

$$\rho_{bf} = 2263.641 - 0.636T(K) \tag{3}$$

3. Results and discussion
3.1 Nanoparticle characterization

Al-Cu alloy nePCMs were first observed by means of TEM as shown in Figure 1a). The nanoparticles are mostly spherical with diameters around 85nm. The presence of an external shell already existing as received was checked, avoiding the need of additional encapsulation steps. These shells have an almost constant thickness ranging from 6 to 8

nm as can be noticed in the micrograph. The encapsulation ratio was calculated as the nuclei volume/total particle volume ratio and a value of 0.532 was obtained.

The nePCMs have also been observed by SEM (Figure 1b)) and more than 3200 diameters have been measured in order to obtain the particle size distribution depicted in Figure 2. It can be noticed that the diameters follow a lognormal trend, centered at 85nm, with particles that can reach up to 300nm.
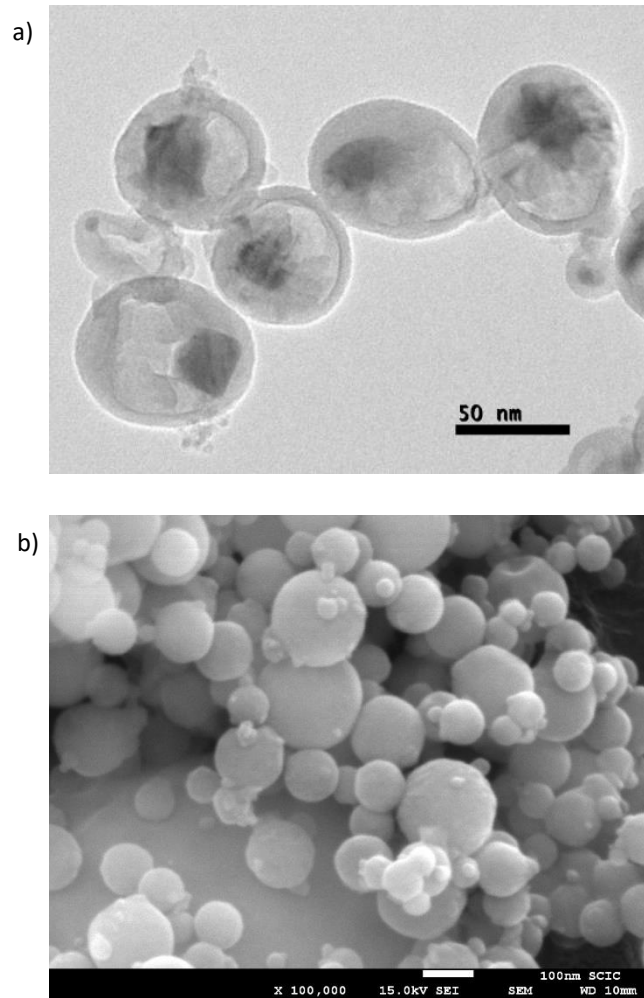

Figure 1.a)TEM and b)SEM micrographs of Al-Cu nePCM
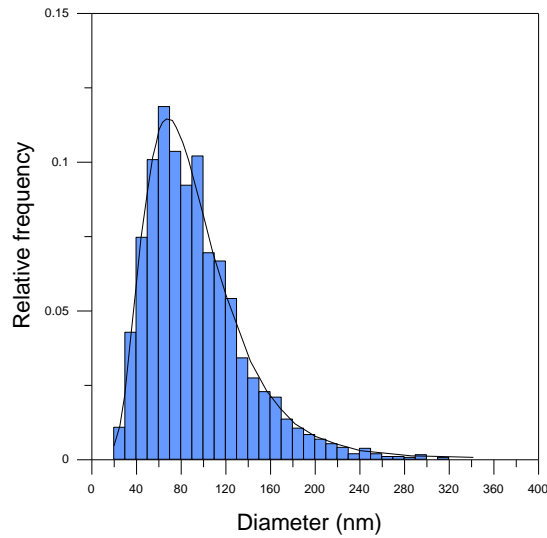
Figure 2.*Nanoparticle size distribution measured by SEM*

EDX analysis confirmed that only aluminium, copper and oxygen were present in the sample as shown in Figure 3 (carbon and nickel are present from the sample holder). It was concluded that nanoparticles are covered by an oxide shell naturally formed during the production process or when exposed to oxygen. As the aluminium is the main component of the alloy and it passivates faster than copper, the shell is composed of aluminium oxide. The natural formation of this covering oxide layer with high melting temperature creates an inert shell that prevents the nucleus material from leaking when melted. From the EDX analysis it was obtained that nanoparticles are composed of 47 wt.% of alumina shell and 53 wt.% of alloy core whose chemical composition is actually 56.6 wt.% Al and 43.4 wt.% Cu (0.754 Al-0.246 Cu molar fraction).
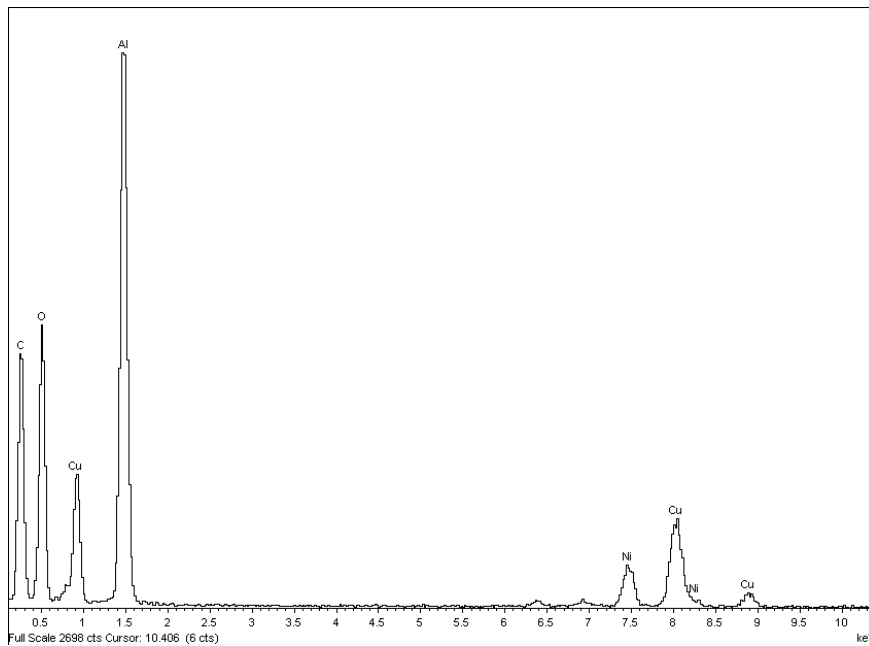

Figure 3.*EDX analysis of Al-Cu nePCM*

3.2 Thermal cycling and latent heat of nePCM and nanofluids

Nanoparticles were submitted to DSC tests from 460ºC to 570ºC in order to obtain the phase change temperature and enthalpy. According to the phase diagram shown in Figure 4a), for the nanoparticle core composition obtained, the liquidus temperature is 547ºC while the solidus temperature is 585ºC. Therefore at 570ºC the core is not fully melted and a solid phase is still remaining together with the liquid phase. Results of DSC test in Figure 4b) provide a melting temperature of 546.74ºC in good agreement with the liquidus temperature available while the crystallisation temperature provided is 540.95ºC. A slight difference between the melting and crystallisation temperatures (supercooling) can be noticed. This difference for Al-Cu alloy is smaller than for other metals because of the remaining solid phase that acts as a nucleation point for heterogeneous crystallisation to occur [31].
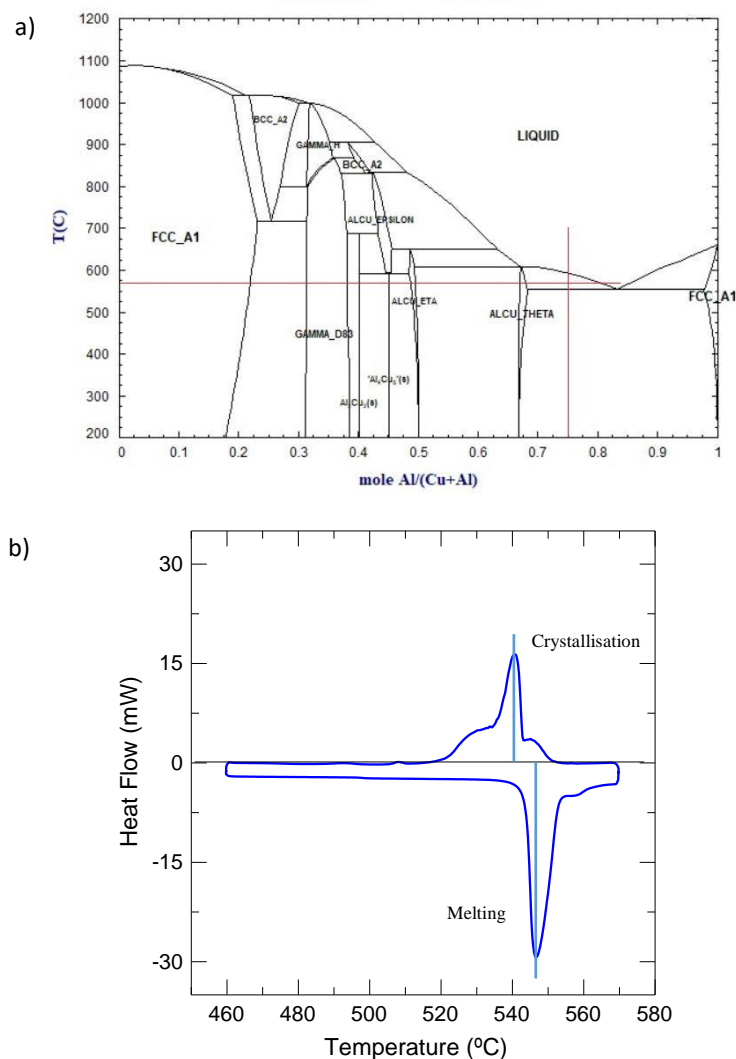

Figure 4._a)Al-Cu phase diagram. b)DSC analysis of Al-Cu nePCM with melting and crystallisation peaks marked_

The encapsulation resistance was tested through the evolution of the phase change enthalpy along 150 thermal cycles. The phase change enthalpy shown in Figure 5 corresponds to the melting peaks, as the width of the peak in the crystallisation is bigger and so it carries higher measurement errors. It is noticeable that there is a period of stabilisation of the nePCM in which the enthalpy apparently decreases during the first cycles, but this is just an artefact caused by a possible non-homogeneous powder-crucible contact. After that period the peaks adjust to their final shape, given that an increase in the values is registered after when the melting process is steady. The results corroborate that after this stabilisation period the melting enthalpy values are rather constant through the cycling and the encapsulating oxide shell stands for the thermal cycling with no change in the DSC curves. It was observed in previous works from the authors [31] that when the shell breaks the phase change enthalpy dramatically decreases, phenomenon not observed in this case.
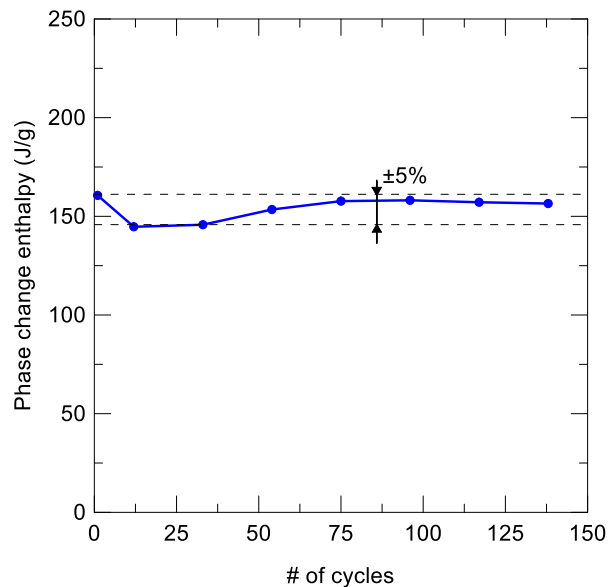

Figure 5.*Evolution of the phase change enthalpy of the nePCM with thermal cycling*

In order to prove the thermal stability of the nePCM when dispersed in the molten salt, a nanofluid with 10% mass loading of nanoparticles was tested. Unlike specific heat, agglomeration of the nePCMs does not have an effect in latent heat, given that it is only dependent on the nuclei material available, i.e., on the mass of nePCMs present. The nanofluid with 10% mass loading was chosen for the tests since the values of phase change enthalpy are higher and thus, the measurement errors are minimized. 55 thermal cycles were performed in the sample and the effect of possible interactions between nanoparticles and base fluid on the performance of the nePCMs was checked through the evolution of the phase change enthalpy. The results of these tests are depicted in Figure 6. In Figure 6a) a negligible displacement of the melting peak is observed for the nePCM immersed in the molten salts. This, along with the stability of the phase change enthalpies observed in Figure 6b) proves that the interaction between the base fluid and

the nanoparticles does not affect their thermal behaviour. Small variations of the phase change enthalpy are observed in Figure 6b). As previously observed for nePCMs, there is a stabilization period in the first few cycles in which the latent heat decreases slightly. After this process, the values are constant within a 5% variability attributed to the measurement technique uncertainty. Therefore, the nePCM behaviour appears to be constant through thermal cycling and can be assumed to keep stable for the next cycles. These results show that the chosen combination of solar salt and Al-Cu nePCM is a compatible one for their use in thermal energy storage applications.
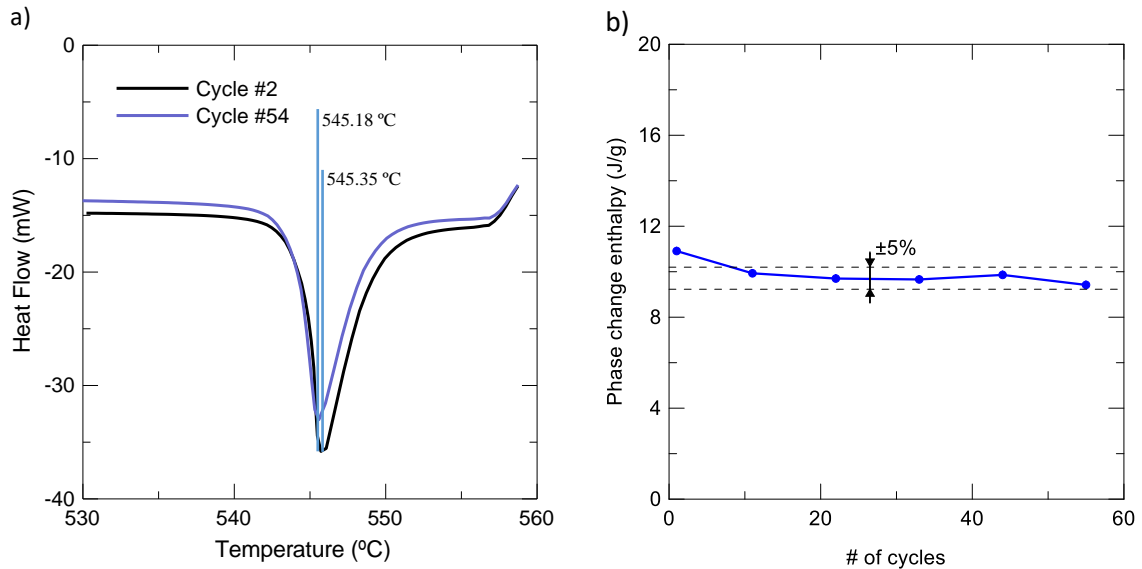

Figure 6. *a)DSC analysis of nanofluid at 10% solid content. b) Evolution of phase change enthalpy of nanofluid with thermal cycling*

3.3 Specific heat

Specific heat capacity of the pure molten salt, nePCM and the molten salt-based nanofluids was measured for different solid contents (0.5%, 1%, 1.5%, 5% and 10%) at three temperatures (300ºC, 350ºC and 400ºC). The absolute values obtained can be found in Table 1, and the specific heat enhancement is plotted in Figure 7. As a general rule the specific heat of the nanofluid is lower than that of the pure molten salt and decreases with solid content due to the lower value for the solid compared to the base fluid. However, an optimum value is achieved a 1.5%. This agrees with results previously found in literature, in which an abnormal enhancement is achieved at solid mass loads around 1% [17, 35]. This phenomenon happens because of the nanoparticle-salt interactions that take place at the nanoparticle surface, mainly ionic exchange reactions, and depends on the available specific surface [24]. This specific surface increases with solid content up to reach a maximum value and then is reduced as the solid content is increased, due to agglomeration.

The same trend is observed for all the temperatures tested and it can be concluded from the absolute values in table 1 that the specific heat is almost constant with temperature and differences lay within the experimental error.
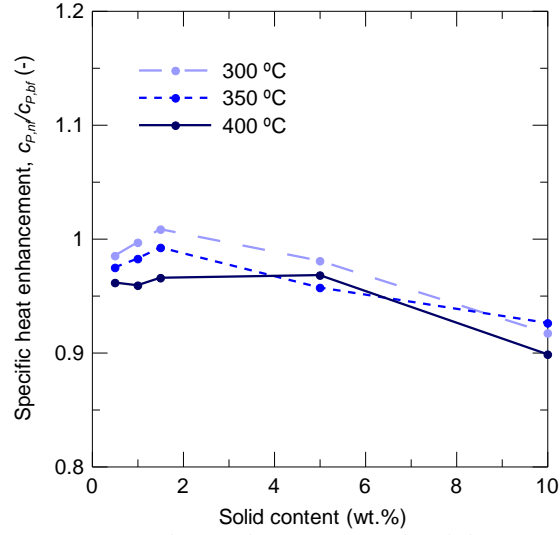
Figure 7. *Evolution of specific heat enhancement with solid content and temperature*

Theoretical values for the specific heat of the nanofluids were calculated applying the mixture rule:

$$c_{P,nf} = w \cdot c_{P,np} + (1-w) \cdot c_{P,bf} \qquad (4)$$

where w is the solid mass fraction, $c_{p,nf}$, $c_{p,np}$ and $c_{p,bf}$ are the specific heat values of the nanofluid, nanoparticle and base fluid respectively.

The relative error, ε_r, between theoretical, $c_{p,th}$, and experimental, $c_{p,exp}$, results were calculated as follow:

$$\varepsilon_r = \frac{|c_{p,th} - c_{p,\exp}|}{c_{p,th}} \cdot 100 \qquad (5)$$

Specific heat of the nanoparticles was calculated according to the composition obtained for the core and shell structure by means of the specific heat values for Al, Cu and Al_2O_3 found in the handbook [36]. Theoretical and experimental results are in good agreement thus corroborating the chemical composition of the nanoparticles.

For the nanofluids, comparing the values obtained from the equation with the ones experimentally measured (Table 1), it can be deduced that the mixture rule fails to predict the abnormal enhancement as well as the values for higher concentrations and temperature, but shows a good agreement in the other conditions.

Table 1. *Specific heat values for nePCM, base fluid and nanofluids at different solid content and temperature*

T (°C)	300			350			400		
Sample	$c_{p,exp}$ (J/g·K)	$c_{p,th}$ (J/g·K)	Error (%)	$c_{p,exp}$ (J/g·K)	$c_{p,th}$ (J/g·K)	Error (%)	$c_{p,exp}$ (J/g·K)	$c_{p,th}$ (J/g·K)	Error (%)
nePCM	0.895	0.898	0.39	0.919	0.920	0.07	0.930	0.941	1.20
Solar Salt (SS)	1.503	1.495	0.56	1.503	1.503	0.02	1.549	1.512	2.46
SS+0.5%Al-Cu	1.481	1.500	1.29	1.465	1.500	2.34	1.489	1.546	3.66
SS+1%Al-Cu	1.498	1.497	0.08	1.477	1.497	1.37	1.486	1.543	3.71
SS+1.5%Al-Cu	1.516	1.494	1.45	1.491	1.494	0.19	1.496	1.540	2.85
SS+5%Al-Cu	1.474	1.473	0.09	1.438	1.474	2.40	1.499	1.518	1.23
SS+10%Al-Cu	1.379	1.442	4.41	1.392	1.445	3.66	1.392	1.487	6.41

3.4 Energy density storage

The total energy density storage of the nanofluids can be expressed as the summation of the sensible heat storage of the mixture and the latent heat storage due to the melting of the nePCM:

$$q_{total} = q_{sensible} + q_{latent} \qquad (6)$$

$$q_{total} = m \cdot c_P \cdot \Delta T + m \cdot \Delta H_f \qquad (7)$$

The energy density storage enhancement provided for the nanofluid compared to the base fluid was calculated by means of the following equation:

$$\Delta q_{total} = \frac{m_{nf}(c_{P,nf} \cdot \Delta T + w \cdot \Delta H_{f,np})}{m_{bf}(c_{P,bf} \cdot \Delta T)} = \frac{\rho_{nf} \cdot V_{nf}(c_{P,nf} \cdot \Delta T + w \cdot \Delta H_{f,np})}{\rho_{bf} \cdot V_{bf}(c_{P,bf} \cdot \Delta T)} \qquad (8)$$

The thermal energy storage enhancement was compared assuming constant mass ($m_{nf} = m_{bf}$) and constant volume ($V_{nf} = V_{bf}$) of the TES material at the same working temperature (close to the phase change). Results can be seen in Figure 8a) and b), where the increase with mass loading of nePCMs is depicted for different temperature ranges in the region of the melting temperature of the nePCM. In both cases, at low concentrations the thermal energy storage decreases due to the decrease of the sensible heat and the small contribution of the latent heat. However, as the solid content increases and thus the latent heat storage contribution becomes of importance the total thermal energy storage is increased. In the graph, it can be also observed that the largest improvements are achieved for the smallest temperature ranges because around the melting temperature the energy stored by the latent heat is higher than the sensible heat. For wider working temperature ranges and high nePCM concentration, sensible heat storage becomes the predominant process and the thermal energy storage enhancement decreases. A maximum enhancement of 10.6% at constant mass basis comparison and 17.8% at constant volume basis comparison can be achieved using the nanofluid containing nanoencapsulated phase change material.
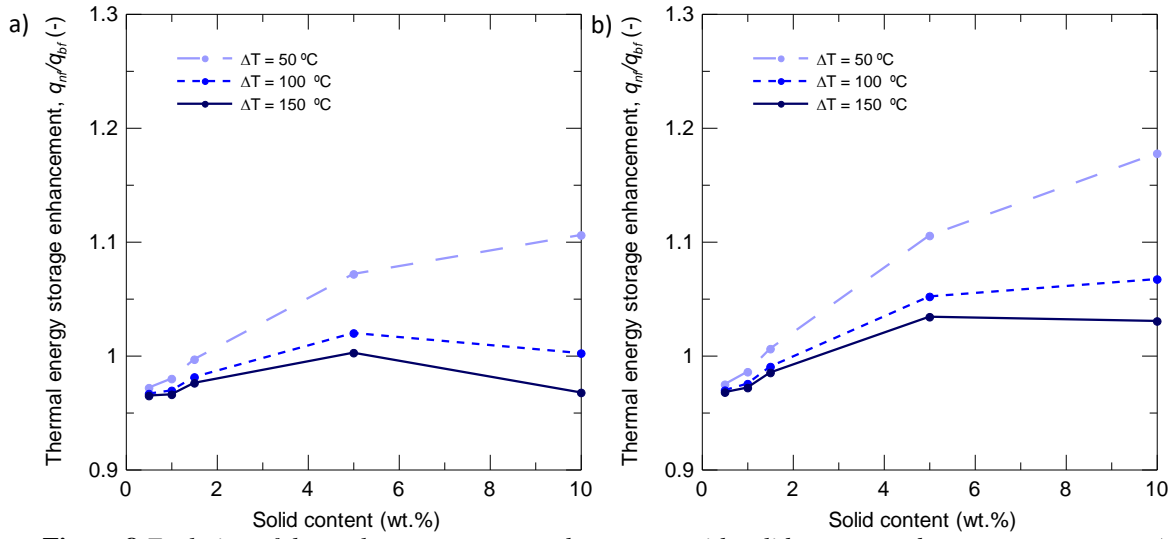
Figure 8. *Evolution of thermal energy storage enhancement with solid content and temperature step at a) constant mass basis and b) constant volume basis comparison*

The enhancement achieved in the thermal energy density storage of the solar salt has an economical and environmental impact. In general, the use of TES systems in CSP plants is attractive because allows to increase annual electricity generation compared to no backup with less greenhouse gas emissions [37]. If TES backup is compared to backup using a natural gas-fired heat transfer fluid heater, the former results in lower annual operation and maintenance costs per unit electricity sold. Also the levelized cost of energy (LCOE) of the plants is less sensitive to variability in nitrate salt pricing than variability in natural gas pricing. Therefore, the increase in the thermal storage and backup capacity can lead to an increase of the electricity generation avoiding the costs due to the need of using natural gas heaters. On the other hand, if the storage capacity of the TES material is higher, the same backup can be obtained reducing the mass or volume of salt thus reducing the cost of the material and the facilities containing it.

3.5 Thermal conductivity and heat transfer

Thermal diffusivity of the salt based nanofluids was experimentally measured at 300°C. Values obtained for the thermal conductivity are shown in Table 2. It can be observed that the addition of nanoparticles increases the thermal conductivity up to an 8.9% maximum. However, the thermal conductivity enhancement decreases with solid content in contrast to that predicted by the Maxwell model. At high concentrations, the abnormal results obtained indicate that the samples are not stable and the agglomeration of nanoparticles leads to a change in the nanofluid composition and properties on the measurement spot thus providing thermal conductivities even lower than the pure salt. The same trend with solid content and temperature can be found in [23].

Theoretical values were calculated by means of the equation for effective conductivity of Maxwell's model [38]:

$$k_{nf} = \frac{k_{np} + 2k_{bf} + 2(k_{np} - k_{bf})\phi}{k_{np} + 2k_{bf} - (k_{np} - k_{bf})\phi} k_{bf} \tag{9}$$

where ϕ is the volume fraction of nanoparticles and k_{nf}, k_{np} and k_{bf} are the thermal conductivities of the nanofluid, nanoparticle and base fluid respectively. Thermal conductivity of the nanoparticles was calculated according to the composition obtained for the core and shell structure by means of the thermal conductivity values for Al, Cu and Al_2O_3 found in the handbook [36] obtaining a result of 166.43 W/m·K.

The relative error, ε_r, between theoretical, k_{th}, and experimental, k_{exp}, results were calculated as follow:

$$\varepsilon_r = \frac{|k_{th} - k_{exp}|}{k_{th}} \cdot 100 \tag{10}$$

It can be also concluded from Table 2 that the Maxwell's model equation can predict the experimental results with less than a 6% of error for lower concentrations. Only for the highest concentrations the error obtained is high confirming the agglomeration of nanoparticles and bad experimental results mentioned above.

Table 2. *Evolution of thermal diffusivity and thermal conductivity with solid content at 300ºC*

Sample	α (mm²/s)	ρ (kg/m³)	Experimental k (W/m·K)	Theoretical k (W/m·K)	Error (%)	k_{nf}/k_{bf}(-)
Solar Salt (SS)	0.155	1899.2	0.441	0.450	1.98	-
SS+0.5%Al-Cu	0.170	1904.4	0.480	0.453	5.92	1.09
SS+1%Al-Cu	0.163	1909.4	0.465	0.457	1.87	1.06
SS+1.5%Al-Cu	0.156	1914.7	0.453	0.460	1.67	1.03
SS+5%Al-Cu	0.148	1951.6	0.424	0.486	12.69	0.96
SS+10%Al-Cu	0.121	2007.3	0.335	0.526	36.39	0.76

Regarding the heat transfer performance of nanofluids, the heat transfer coefficient (h) can be calculated from the Nusselt number:

$$Nu = \frac{h \cdot D}{k} \tag{11}$$

For laminar flow regimen the Nusselt number is considered to be constant ($Nu = 3.66$ for circular pipes) and thus the increase in the heat transfer coefficient is directly proportional to the thermal conductivity enhancement. However, for turbulent flow regime the Nusselt number depends on the Reynolds and Prandtl numbers which depend in turn on the thermal conductivity, specific heat and viscosity. Although a more in depth analysis is needed to evaluate the heat transfer performance, the use of nanofluids with enhanced thermal conductivity has proved to increase the heat transfer coefficient when working at constant Reynolds number [39]. Therefore the increase in the thermal conductivity of molten salt based nanofluids can be beneficial to improve its heat transfer performance under some working conditions.

An approach to this analysis is shown in Table 3, where the heat transfer coefficient ratio has been used as the figure of merit to evaluate the heat transfer performance. Thus, for a turbulent flow with the heat transfer coefficient described by the Dittus-Boelter equation, the ratio has been evaluated as:

$$\frac{h_{nf}}{h_{bf}} = \frac{Mo_{nf}}{Mo_{bf}} = \left(\frac{\rho_{nf}}{\rho_{bf}}\right)^{0.8} \left(\frac{c_{p_{nf}}}{c_{p_{bf}}}\right)^{0.4} \left(\frac{\mu_{nf}}{\mu_{bf}}\right)^{-0.4} \left(\frac{k_{nf}}{k_{bf}}\right)^{0.6} \tag{12}$$

where Mo is the Mouromtseff number [40], used in literature as an indicator of the heat transfer coefficient enhancement of nanofluids based on their physical parameters [41,42].

In order to resolve Equation 12, the density has been calculated from the density of pure components, specific heat and conductivity have been measured experimentally (Table 1 and Table 2), and the viscosity has been theoretically evaluated using the Einstein equation [43]. In Table 3 it is observed that the heat transfer performance is improved for the nanofluids with the smaller nePCM loads (0.5%wt., 1%wt. and 1.5%wt.) but it actually decreases for the higher ones. However, further research is needed as the Einstein equation is valid for dilute suspensions but usually fails to predict the viscosity of high concentrated samples.

Table 3.*Evolution of heat transfer performance with solid content at 300ºC.*

Sample	ρ (kg/m³)	c_p (J/gK)	k (W/mK)	μ (mPa·s)	Mo_{nf}/Mo_{bf}
Solar Salt (SS)	1899.21	1.503	0.441	3.650	-
SS+0.5%Al-Cu	1904.41	1.481	0.480	3.673	1.046
SS+1%Al-Cu	1909.42	1.498	0.465	3.697	1.031
SS+1.5%Al-Cu	1914.72	1.516	0.453	3.720	1.018
SS+5%Al-Cu	1951.63	1.474	0.424	3.887	0.966
SS+10%Al-Cu	2007.26	1.379	0.335	4.139	0.814

4. Conclusions

A nePCM consisting on an Al-Cu metallic alloy nanoparticles with core-shell structure, in which the shell is a naturally formed layer of aluminium oxide, has been tested for its use in thermal energy storage applications. The nanoparticles have been proved to remain unaltered through thermal cycling, keeping their latent heat characteristics and resisting working temperatures common for the solar energy industry.

Nanofluids based on Solar Salt and Al-Cu nePCM with different concentrations have been characterized and compared to the base fluid alone in terms of specific heat, total thermal energy storage and thermal conductivity. Variations in the specific heat of the nanofluids have been observed, presenting in general a decrease of the values respect to Solar Salt, as expected from the mixture rule. However, although the sensible heat storage decreases the total energy storage can be increased thanks to the contribution of the latent heat storage of the nePCM. As the solid content is increased, the latent heat storage can overcome the sensible heat decrement and maximum energy storage of 10.6% at constant mass basis and 17.8% at constant volume basis can be achieved at 10 wt.% of nePCM for a working temperature range of 50ºC around the melting point. Besides, the addition of nanoparticles can increase the thermal conductivity of the nanofluid and improve its heat transfer performance under some particular conditions.

In conclusion, a nanofluid based on molten solar salt containing Al-Cu nePCM can be used as improved TES material showing chemical compatibility with the solar salt through thermal cycling. This technology has a positive economic and environmental impact.

References

1. Alva, G., Lin, Y., Fang, G. An overview of thermal energy storage systems. Energy 144 (2018) 341-378.

2. Mahian, O., Kianifar, A., Kalogirou, S.A., Pop, I., Wongwises, S.A review of the applications of nanofluids in solar energy. International Journal of Heat and Mass Transfer 57 (2013) 582–594.

3. Mondragon, R., Navarrete, N., Gimeno-Furio, A., Hernandez, L., Cabedo, L., Julia, J.E. Advances in New Heat Transfer Fluids From Numerical to Experimental Techniques. Chapter 11- New High-Temperature Heat Transfer and Thermal Storage Molten Salt–Based Nanofluids Preparation, Stabilization, and Characterization. Taylor & Francis Group, LLC. 2017

4. Pfleger, N., Bauer, T., Martin, C., Eck, M., Wörner, A.. Thermal energy storage – overview and specific insight into nitrate salts for sensible and latent heat storage. Beilstein Journal of Nanotechnolgy 2015, 6, 1487–1497.

5. Gasia, J., Miró, L., Cabeza, L.F., Review on system and materials requirements for high temperature thermal energy storage. Part 1: General requirements. Renewable and Sustainable Energy Reviews 75 (2017) 1320-1338.

6. Zhang, Z., Alva, G., Gu, M., Fang, G., Experimental investigation on neoctadecane/ polystyrene/expanded graphite composites as form-stable thermal energy storage materials. Energy 157 (2018) 625-632.

7. Zhang, H., Kong, W., Tan, T., Baeyens, J., High-efficiency concentrated solar power plants need appropriate materials for high-temperature heat capture, conveying and storage. Energy 139 (2017) 52-64.

8. Kahwaji, S., Johnson, M.B., Kheirabadi, A.C., Groulx, D., White, M.A., A comprehensive study of properties of paraffin phase change materials for solar

thermal energy storage and thermal management applications. Energy 162 (2018) 1169-1182.

9. Serrano-López, R., Fradera, J., Cuesta-López, S. Molten salts database for energy applications. Chemical Engineering and Processing 73 (2013) 87–102.

10. Bonk, A., Sau, S., Uranga, N., Hernaiz, M., Bauer, T. Advanced heat transfer fluids for direct molten salt line-focusing CSP plants. Progress in Energy and Combustion Science 67 (2018) 69-87.

11. Muñoz-Sánchez, B., Nieto-Maestre, J., Iparraguirre-Torres, I., García-Romero, A., Sala-Lizarraga, J.M. Molten salt-based nanofluids as efficient heat transfer and storage materials at high temperatures. An overview of the literature. Renewable and Sustainable Energy Reviews 82 (2018) 3924–3945.

12. Riazi, H., Murphy, T., Webber, G.B., Atkin, R., MostafaviTehrani, S.S., Taylor, R.A. Specific Heat Control of Nanofluids: a Critical Review. International Journal of Thermal Sciences107, 25-38 (2016).

13. Taylor, R., Coulombe, S., Otanicar, T., Phelan, P., Gunawan, A., Lv, W., Rosengarten, G., Prasher, R., Tyagi, H., "Small particles, big impacts: A review of the diverse applications of nanofluids", Journal of Applied Physics, 113, 011301 (2013).

14. Shin, D., Banerjee, D. Experimental Investigation of Molten Salt Nanofluid for Solar Thermal Energy Application. 8th Thermal Engineering Joint Conference AJTEC (2011).

15. Tiznobaik, H., Shin, D. Enhanced specific heat capacity of high-temperature molten salt-based nanofluids. International Journal of Heat and Mass Transfer 57, 542-548 (2013).

16. Dudda, B., Shin, D. Effect of nanoparticle dispersion on specific heat capacity of a binary nitrate salt eutectic for concentrated solar power applications. International Journal of Thermal Sciences 69, 37-42 (2013).

17. Andreu-Cabedo, P., Mondragon, R., Hernandez, L., Martinez-Cuenca, R., Cabedo, L., Julia, J.E. Increment of specificheatcapacity of solar saltwith SiO2 nanoparticles. Nanoscale Research Letters 9, 582–592 (2014).

18. Lasfargues, M., Stead, G., Amjad, M., Ding, Y., Wen, D. In Situ Production of Copper Oxide Nanoparticles in a Binary Molten Salt for Concentrated Solar Power Plant Applications. Materials 10, 537 (2017).

19. Hu, Y., He, Y., Zhang, Z., Wen, D. Effect of Al2O3 nanoparticle dispersion on the specific heat capacity of a eutectic binary nitrate salt for solar power applications. Energy Conversion and Management 142, 366–373 (2017).

20. Qiao, G., Lasfargues, M., Alexiadis, A., Ding Y. Simulation and experimental study of the specific heat capacity of molten salt based nanofluids. Applied Thermal Engineering 111, 1517–1522 (2017).

21. Luo, Y., Du, X., Awad, A., Wen, D. Thermal energy storage enhancement of a binary molten salt via in-situ produced nanoparticles. International Journal of Heat and Mass Transfer 104, 658–664 (2017).

22. Chieruzzi, M., Cerritelli, G.F., Miliozzi, A., Kennya, J.M., Torre, L. Heat capacity of nanofluids for solar energy storage produced by dispersing oxide nanoparticles

in nitrate salt mixture directly at high temperature. Solar Energy Materials and Solar Cells 167, 60–69 (2017).

23. Awad, A., Navarro, H., Ding, Y., Wen, D. Thermal-physical properties of nanoparticle-seeded nitrate molten salts. Renewable Energy 120 (2018) 275-288.

24. Mondragón, R., Juliá, J.E., Cabedo, L., Navarrete, N. On the relationship between the specific heat enhancement of salt-based nanofluids and the ionic exchange capacity of nanoparticles. Scientific Reports (2018) 8:7532.

25. Paul, T.C., Morshed, A.K.M.M., Fox, E.B., Khan, J.A.. Enhanced thermophysical properties of NEILs as heat transfer fluids for solar thermal applications. Applied Thermal Engineering 110 (2017) 1–9.

26. Nieto de Castro, C.A., Murshed, S.M.S., Lourenço, M.J.V., Santos, F.J.V., Lopes, M.L.M., França, J.M.P.. Enhanced thermal conductivity and specific heat capacity of carbon nanotubes ionanofluids. International Journal of Thermal Sciences 62 (2012) 34-39.

27. Hong, Y., Ding, S., Wu, W., Hu, J., Voevodin, A.A.,Gschwender, L, Snyder, E., Chow, L., Su, M. Enhancing Heat Capacity of Colloidal Suspension Using Nanoscale Encapsulated Phase-Change Materials for Heat Transfer. ACS Applied Materials and Interfaces 2, 1685–1691, 2010.

28. Hong, Y., Wu, W., Hu, J., Zhang, M., Voevodin, A.A., Chow, L., Su, M. Controlling super-cooling of encapsulated phase change nanoparticles for enhanced heat transfer. Chemical Physics Letters 504 (2011) 180–184.

29. Cingarapu, S., Singh, D., Timofeeva, E.V., Moravek, M.R. Nanofluids with encapsulated tin nanoparticles for advanced heat transfer and thermal energy storage. International Journal of Energy Research 2014; 38:51–59.

30. Cingarapu, S., Singh, D., Timofeeva, E.V., Moravek, M.R., "Use of encapsulated zinc particles in a eutectic chloride salt to enhance thermal energy storage capacity for concentrated solar power", Renewable Energy, 80, 508-516 (2015).

31. Navarrete, N., Gimeno-Furio, A., Mondragon, R., Hernandez, L., Cabedo, L., Cordoncillo, E., Julia, J.E., "Nanofluid based on self-nanoencapsulated metal/metal alloys phase change materials with tuneable crystallisation temperature", Scientific Reports, 7, 17580 (2017).

32. Milián, Y.E., Gutiérrez, A., Grágeda, M., Ushak, S. A review on encapsulation techniques for inorganic phase change materials and the influence on their thermophysical properties. Renewable and Sustainable Energy Reviews 73 (2017) 983–999.

33. Jamekhorshid, A., Sadrameli, S.M., Farid, M.. A review of microencapsulation methods of phase change materials (PCMs) as a thermal energy storage (TES) medium. Renewable and Sustainable Energy Reviews 31 (2014) 531–542.

34. Ferrer, G., Barreneche, C., Solé, A., Martorell, I., Cabeza, L.F., "New proposed methodology for specific heat capacity determination of materials for thermal energy storage (TES) by DSC", Journal of Energy Storage, 11, 1-6 (2017).

35. Hentschke, R. On the specific heat capacity enhancement in nanofluids. Nanoscale Research Letters 11, 88 (2016).

36. 1873.Perry, R.H., Green, D.W. Perry's Chemical Engineers' Handbook, 7th Edition. McGraw-Hill. 2001.

37. Wagner, S.J., Rubin, E.S. Economic implications of thermal energy storage for concentrated solar thermal power. Renewable Energy 61 (2012) 81-95.

38. J.C. Maxwell, A Treatise on Electricity and Magnetism, Clarendon Press, Oxford, UK.

39. Martínez-Cuenca, R., Mondragón, R., Hernández, L., Segarra, C., Jarque, J.C., Hibiki, T., Juliá, J.E. Forced-convective heat-transfer coefficient and pressure drop of water-based nanofluids in a horizontal pipe. Applied Thermal Engineering 98 (2016) 841–849.

40. W. Yu, E.V. Timofeeva, D. Singh, D.M. France, R.K. Smith, Investigations of heat transfer of copper-in-Therminol 59 nanofluids, International Journal of Heat Mass Transfer 64 (2013) 1196–1204.

41. Minea, A.A., Moldoveanu, M.G., Studies on Al2O3, CuO, and TiO2 water-based nanofluids: A comparative approach in laminar and turbulent flow. Journal of Engineering Thermophysics 26 (2017) 231-301.

42. Gimeno-Furio, A., Navarrete, N., Mondragon, R., Hernandez, L., Martinez-Cuenca, R., Cabedo, L., Julia, J.E., Stabilization and characterization of a nanofluid based on a eutectic mixture of diphenyl and diphenyl oxide and carbon nanoparticles under high temperature conditions. International Journal of Heat and Mass Transfer 113 (2017) 908-913.

43. Einstein, A., Eine neue Bestimmung der Moleküldimensionen. Annalen der Physik, 19 (1906) 289-306.